Supplementary Material.

Differences in protein concentration dependence for nucleation and elongation in light chain amyloid formation.

Luis M. Blancas-Mejía[†], Pinaki Misra[†], Marina Ramirez-Alvarado[*,†,‡].

[†]Department of Biochemistry and Molecular Biology; [‡]Department of immunology, Mayo Clinic, Rochester, MN 55905 ramirezalvarado.marina@mayo.edu

Table S1. Crystallographic data collection and refinement statistics (molecular replacement).

Data collection [a]	
Space group	P 1
Cell dimensions	
a,b,c	38.46, 42.12, 65
α,β,γ	80.66, 86.02, 63.02
Resolution (Å)	37.10–1.90 (37.11–1.90) [b]
Unique reflections	24,891 (1,477)
Wilson B-factor	23.7
Rmerge (%)	6.0 (15.4)
I/sI	8.13 (1.90)
Completeness (%)	88.1 (37.10-1.90)
Redundancy	90.7
Refinement	
Reflections used	24,891 (1,447)
Rwork/Rfree (%)	21.1/23.5 (28.4/29.6)
Atom number	
Number of Protein atoms	9351
Number of solvent atoms	847
Zn	7
r.m.s.[c] deviations	
Average B-factors	26
Bond length(Å))	0.013
Bond angles(°)	1.49
Bond lengths	0.006
Bond angles	1.236
MolProbity clashscore	12.11
%Ramachandran outliers	0
%Rotamer outliers	0

[a] One crystal was used to determine each structure.

[b] Values in parentheses are for highest-resolution shell.

[c] RMSDs root mean square.

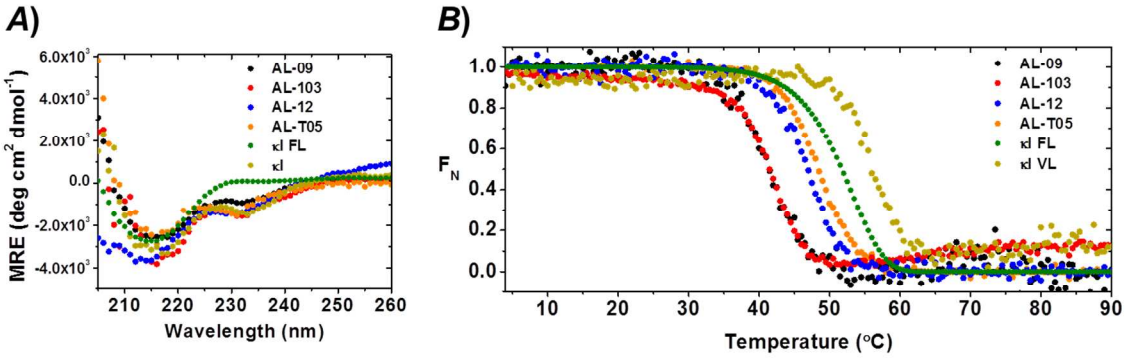

Figure S1. Far UV-CD spectra (*A*) and thermal unfolding analysis *(B)* of AL-09 (*Black)*; AL-103 (*red*); AL-12 (*blue*); AL-T05 (*orange*); κI FL (*green*); and κI (*brown*). All proteins display b-sheet structure with the characteristic two minima (235 and ~217 nm) for these proteins. Experimental conditions were as follows: 20 µM protein in 10 mM Tris-HCl, pH 7.4. Far UV-CD spectra were acquired at 4°C. Thermal denaturation experiments were performed from 4–90°C at a rate of 0.5°C min^{-1}.(Modified from Blancas et al. 2016[30])

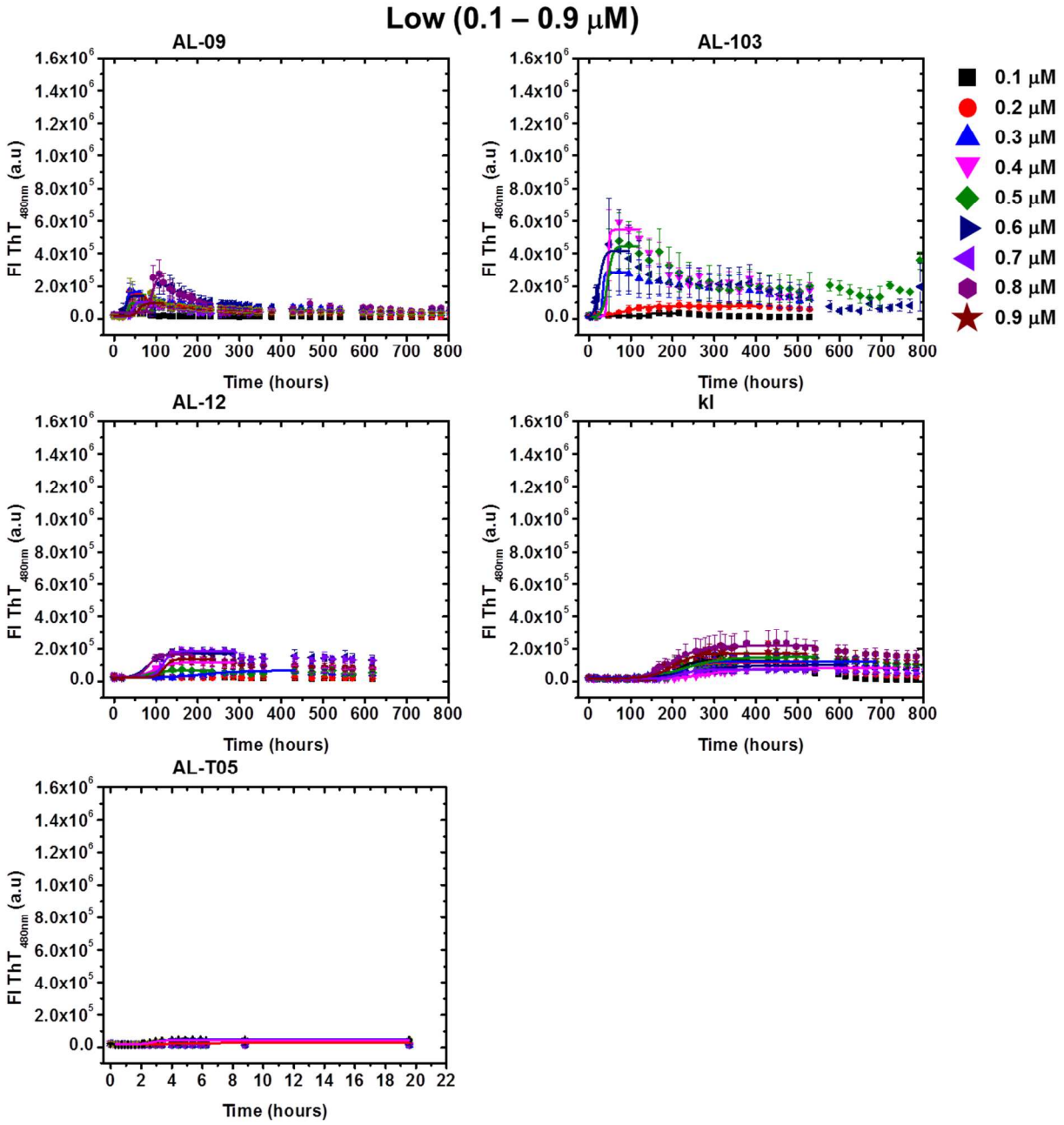

Figure S2. *De novo* fibril formation kinetics at low-concentration regime (0.1 uM-0.9 μM) for AL-09, AL-103, AL-12, κI, and AL-T05. Continuous lines represent the best fitting to Eq. 1. Error bars are from triplicates.

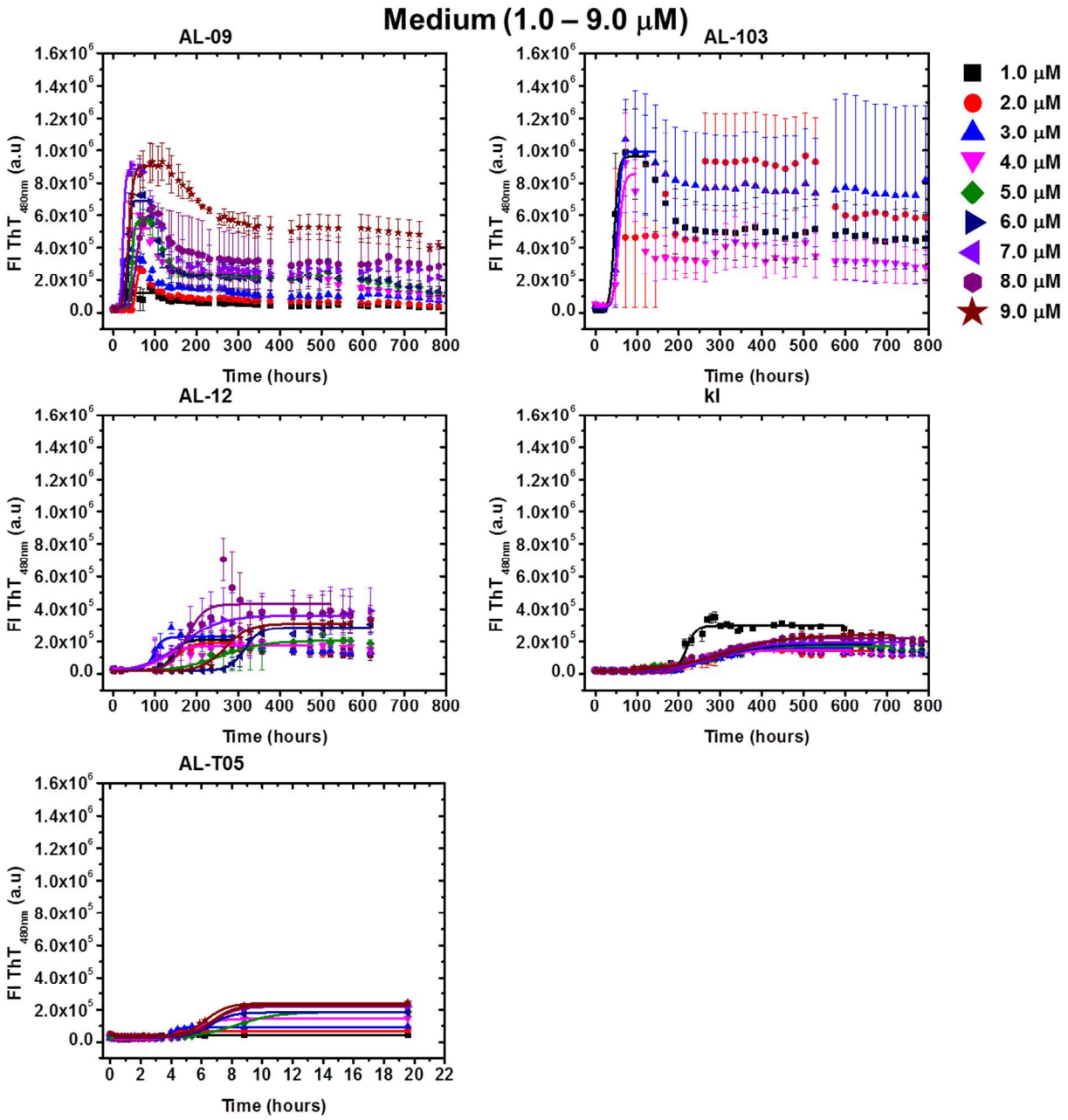

Figure S3. *De novo* fibril formation kinetics at medium concentration regime (1-9 μM) for AL-09, AL-103, AL-12, κI, and AL-T05. Continuous lines represent the best fitting to Eq. 1. Error bars are from triplicates.

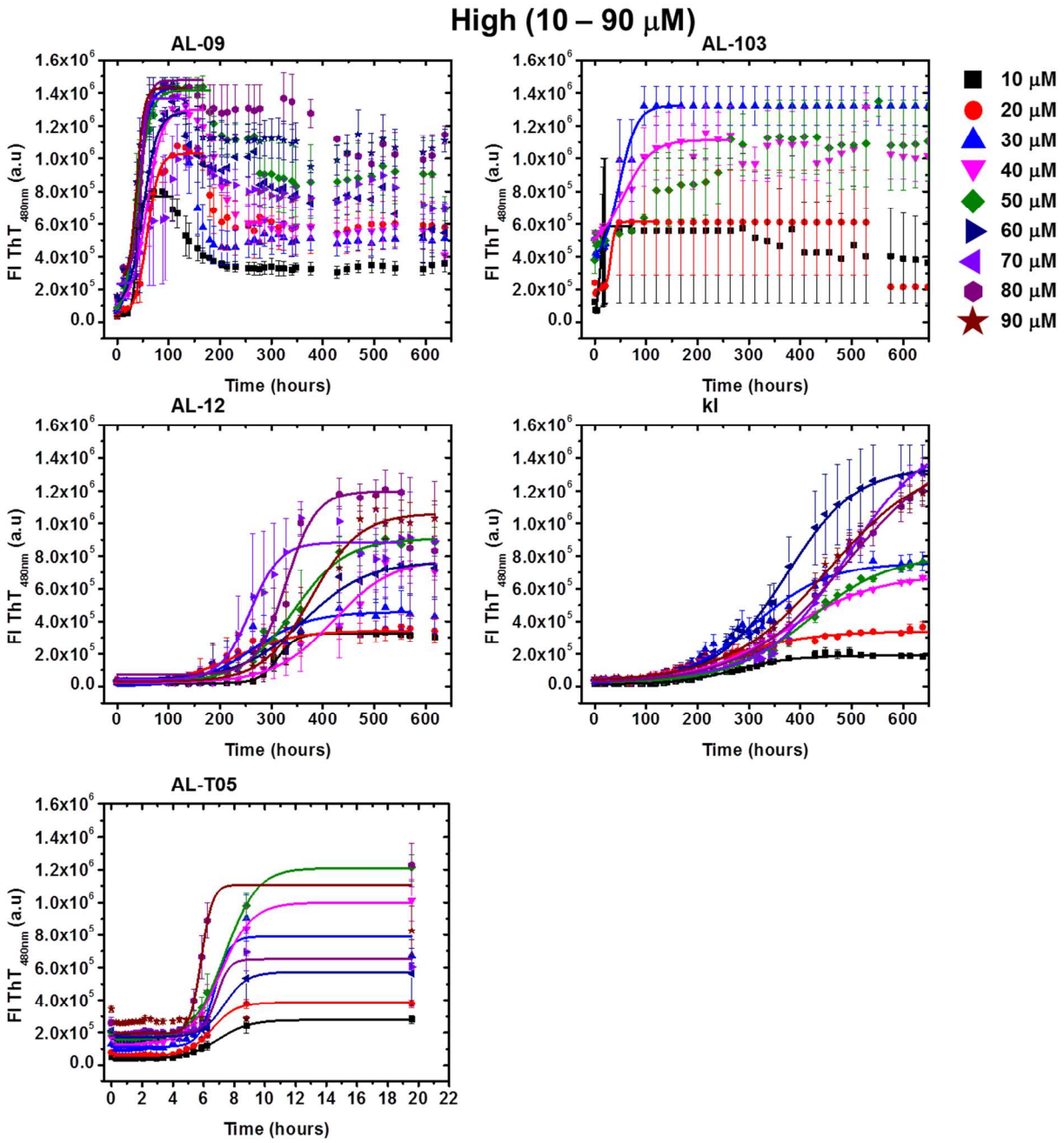

Figure S4. *De novo* fibril formation kinetics at high-concentration regime (10-90 μM) for AL-09, AL-103, AL-12, κI, and AL-T05. Continuous lines represent the best fitting to Eq. 1. Error bars are from triplicates.

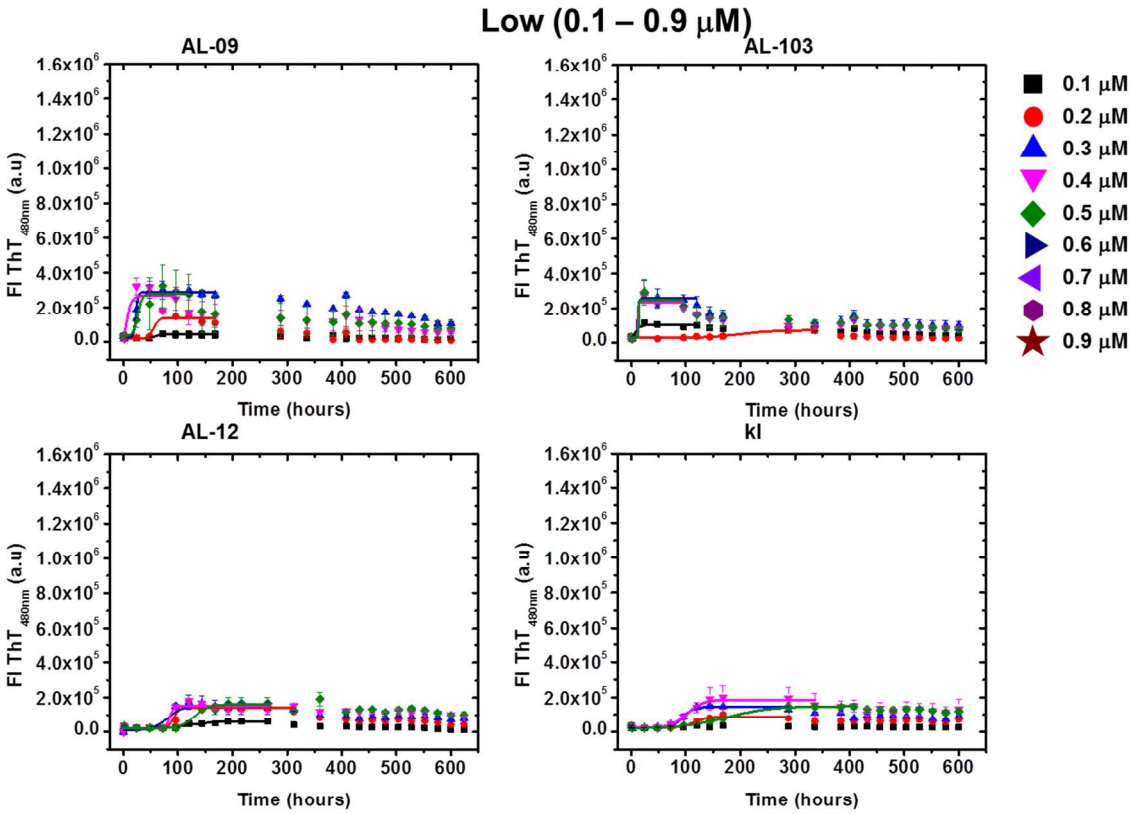

*Experiment with 1% seeds

Figure S5. Fibril formation kinetics in presence of 1% seeds, at low-concentration (0.1-0.9 μM) regime for AL-09, AL-103, AL-12, and κI. Continuous lines represent the best fitting to Eq. 1. Error bars are from triplicates.

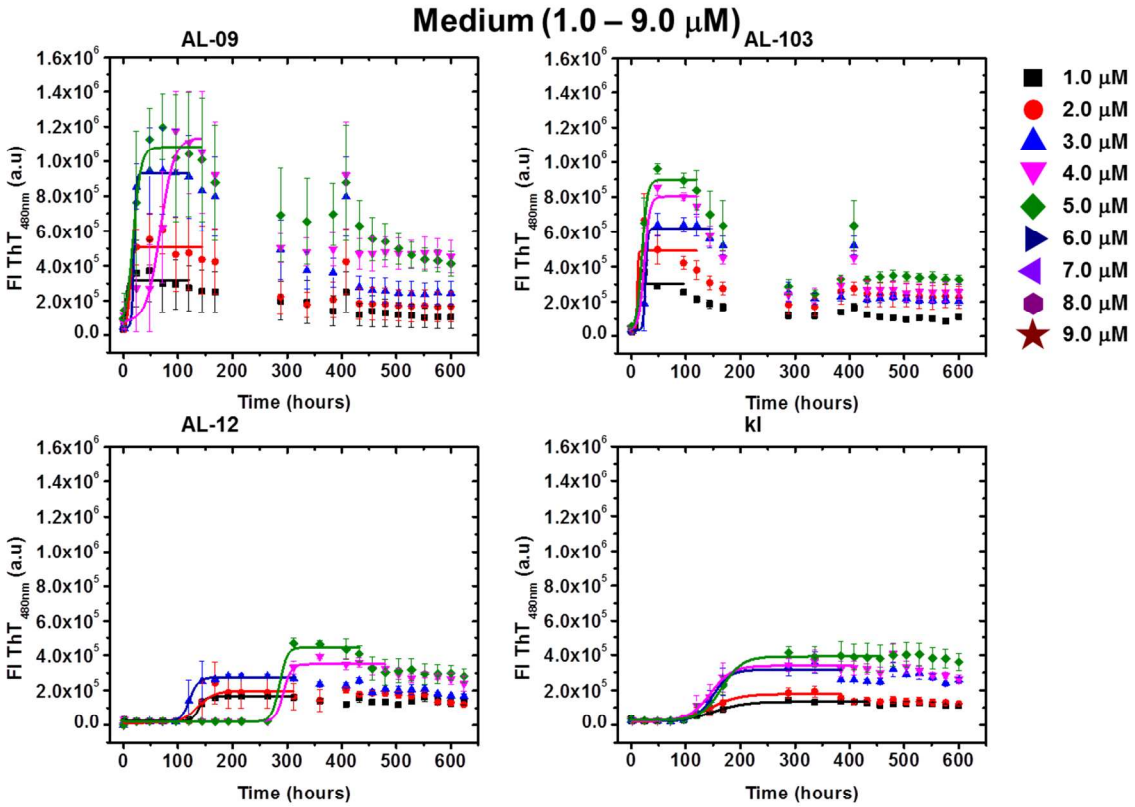

*Experiment with 1% seeds

Figure S6. Fibril formation kinetics in presence of 1% seeds, at medium concentration (1-9 μM) regime for AL-09, AL-103, AL-12, and κI. Continuous lines represent the best fitting to Eq. 1. Error bars are from triplicates.

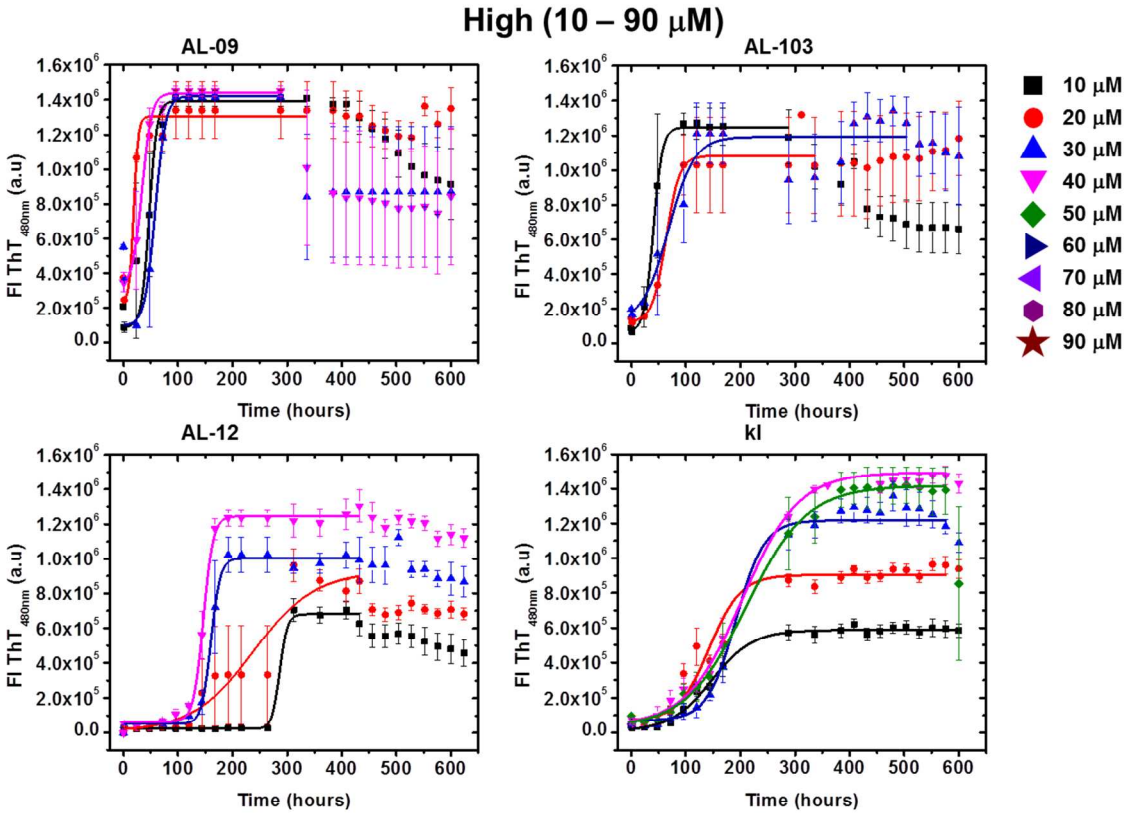

*Experiment with 1% seeds

Figure S7. Fibril formation kinetics in presence of 1% seeds, at high concentration (10-90 μM) regime for AL-09, AL-103, AL-12, and κI. Continuous lines represent the best fitting to Eq. 1. Error bars are from triplicates.

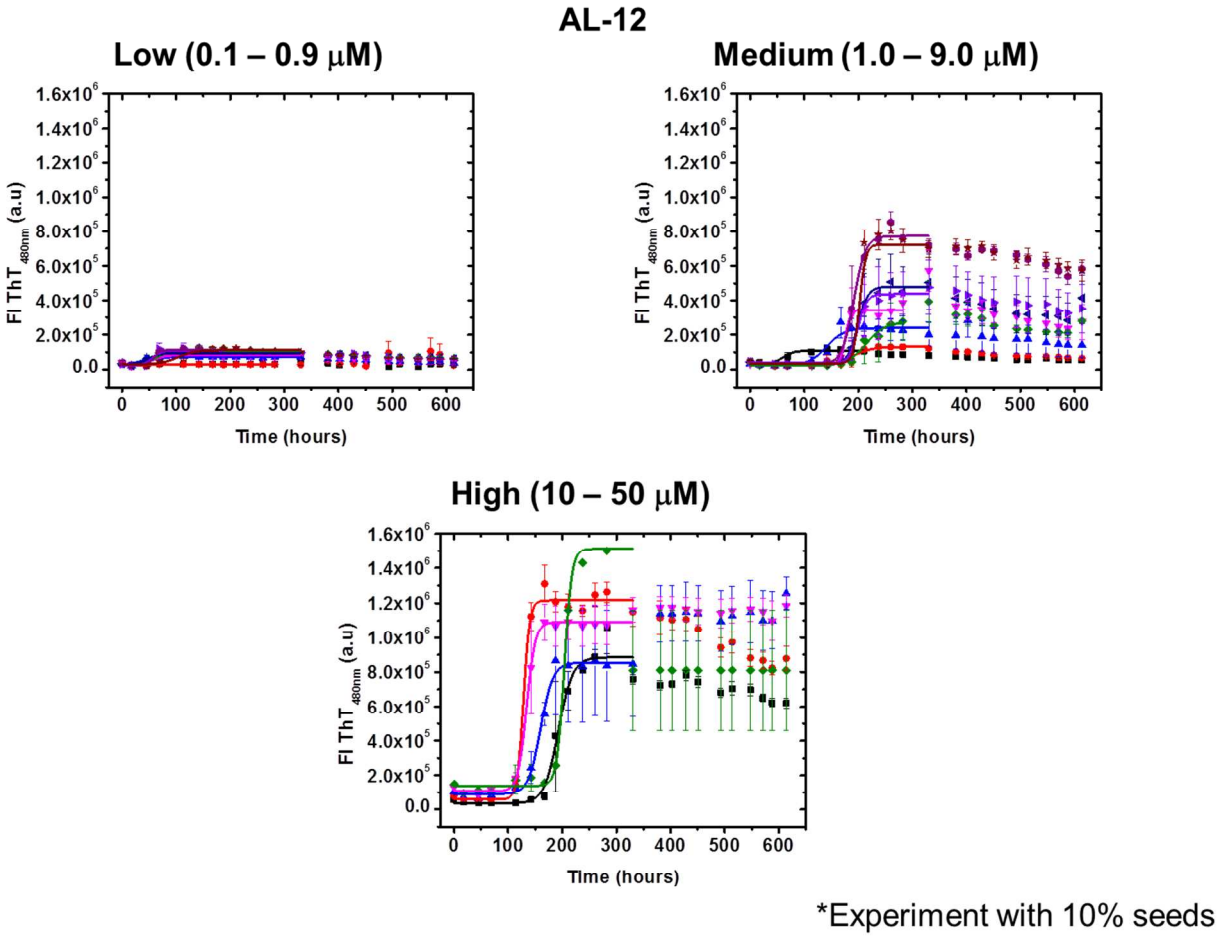

Figure S8. Fibril formation kinetics in presence of 10% seeds for AL-12. Continuous lines represent the best fitting to Eq. 1. Error bars are from triplicates.